Journal of Macromolecular Science, Part A
Publication details, including instructions for authors and subscription information:
http://www.informaworld.com/smpp/title~content=t713597274

Synthesis and Properties of Narrow-sized Spherical Aramides Nanoparticles Containing Pyridine and their Copper (II) Complexes

Hammed H. A. M. Hassan[a]; Amel F. Elhusseiny[a]; Amr M. Sweyllam[b]
[a] Chemistry Department, Faculty of Science, Alexandria University, Moharrem Bee, Alexandria, Egypt
[b] Physics Department, Faculty of Science, Alexandria University, Moharrem Bee, Alexandria, Egypt

Online publication date: 19 November 2010

To cite this Article Hassan, Hammed H. A. M. , Elhusseiny, Amel F. and Sweyllam, Amr M.(2011) 'Synthesis and Properties of Narrow-sized Spherical Aramides Nanoparticles Containing Pyridine and their Copper (II) Complexes', Journal of Macromolecular Science, Part A, 48: 1, 73 — 89
To link to this Article: DOI: 10.1080/10601325.2011.528312
URL: http://dx.doi.org/10.1080/10601325.2011.528312

Journal of Macromolecular Science, Part A: Pure and Applied Chemistry (2011) **48**, 73–89

ISSN: 1060-1325 print / 1520-5738 online
DOI: 10.1080/10601325.2011.528312

Synthesis and Properties of Narrow-sized Spherical Aramides Nanoparticles Containing Pyridine and their Copper (II) Complexes

HAMMED H. A. M. HASSAN[1,*], AMEL F. ELHUSSEINY[1] and AMR M. SWEYLLAM[2]

[1]*Chemistry Department, Faculty of Science, Alexandria University, Moharrem Bee, Alexandria, Egypt*
[2]*Physics Department, Faculty of Science, Alexandria University, Moharrem Bee, Alexandria, Egypt*

Received February 2010, Accepted June 2010

We report the preparation of narrow-sized well-separated spherical aramides nanoparticles containing pyridine using the precipitation polymerization method. The average diameter of the particles ranges from 50–98 nm. Particles of pyridine containing polymers exhibited large diameter compared to their phenylene counterpart. Symmetric meta-polymers showed relatively higher η_{inh} and thermal stability and thus higher degree of polymerization than their nonsymmetrical counterparts. Incorporation of Copper (II) ions into these polymers furnished copper-polymer complexes in a (1:2) ratio and the reported structures are proposed on the basis of their IR, UV, ESR and elemental analysis data. The ERS spectra of the complexes exhibited typical axial spectra with $g_{//}$ and $g_{\perp}$ features and the data indicated that the copper site has a d_{x2-y2} ground state, characteristic of square planar or elongated octahedral stereochemistry. The incorporation of copper into aramides backbones significantly improved their optical and thermal properties. The dc electrical conductivity of polymeric copper complexes revealed different behaviors and it is obvious that the prepared pyridine-containing polymers exhibited higher σ values compared to their phenylene analogues. These types of nano-sized aramides and their copper complexes may find some applications as new semiconducting nanoparticles.

Keywords: Nanoparticles, aramides, morphology, structure-property relations, polymer copper complex

1 Introduction

Wholly aromatic polyamides are synthetic polyamides in which at least 85% of amide groups are bound directly to two aromatic rings (1). Aramides are considered to be high-performance materials due to their superior thermal and mechanical properties, which make them useful for advanced technologies. The commercial production of the industrially important polyamide fiber (*Nomex*) **1**; [poly (*m*-phenyleneisophthalamide)] (Fig. 1) by *Du Pont* Company, had opened the door for further efforts focused on chemically modifying the composition of these materials for further industrial applications. The preparation and processing of poly (*p*-phenyleneterephthalamide) **2** led to commercialization of the *para* product polyamide fiber (*Kevlar*).

The wholly aromatic structure with all-*para* substitutions creates stiff rod-like macromolecules, having a high cohesive energy and a high crystallization tendency due to the very favorable intramolecular hydrogen bonds. *Kevlar* fibers can be transformed into materials and composites having superior thermal and mechanical resistance. Aromatic polyamides with all-*meta* orientation in the phenylene ring, on the other hand, have less linear structures and a concomitant reduction in its cohesive energy and crystallization tendency. Thus, **1** is a high-performance polymer, with high thermal and mechanical resistance. Aramides **1**, **2** and also poly(*m*−phenyleneterephthalamide) **3** have been recognized as the most successful aromatic polymer materials due to their extensive applications in high-tech industry (2–6). However, aromatic polyamides are insoluble in conventional solvents but soluble in strong acids such as sulfuric acid and hydrochloric acid. These characteristics make it difficult to mold polyamide materials in secondary processes. Various structural changes have been introduced in the aramid backbone to obtain different properties and for different applications (7–14). A remarkable feature of

*Address correspondence to: Hammed H. A. M. Hassan, Chemistry Department, Faculty of Science, Alexandria University, P. O. Box 2-Moharrem Bee, Alexandria-21568, Egypt. Tel: +2 012 5888 595; Fax: +203 39 11 794; E-mail: hassan10@safwait.com

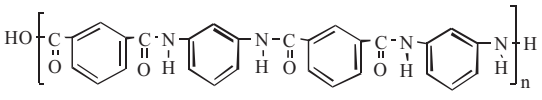

1 poly (*m*-phenyleneisophthalamide) "Nomex"

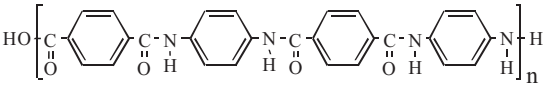

2 poly(*p*-phenyleneterephthalamide) "Kevlar"

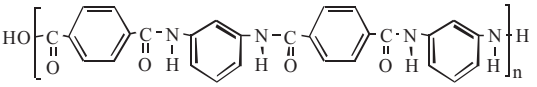

3 poly (*m*-phenylene terephthalamide)

Fig. 1. The most applied aromatic polyamide materials in high-tech industry.

modified aramides derived from 2,6-diaminopyridine and 2,6-pyridinedicarboxylic acid, is their fold into stable single helical conformations in a variety of solvents (15). These helices have the ability to entwine and form double helical dimmer (16), (Fig. 2) which is, in its turn, stabilized by direct interactions between the two strands. The conformation of such polymers can be easily controlled leading to either linear strand or refolding into a different helix. Such conformation control represents the key step toward the development of mechanical molecular devices (17).

Polymer particles with a narrow particle size distribution have received much attention for possible new applications, such as spacers for display, medical carriers, and chromatographic media (18–23). Recently, we reported the chemistry of nanometer-sized rod-like pyridine-containing polyesteramids and their copper (II) complexes (24). In this paper, we report the preparation of aramides containing

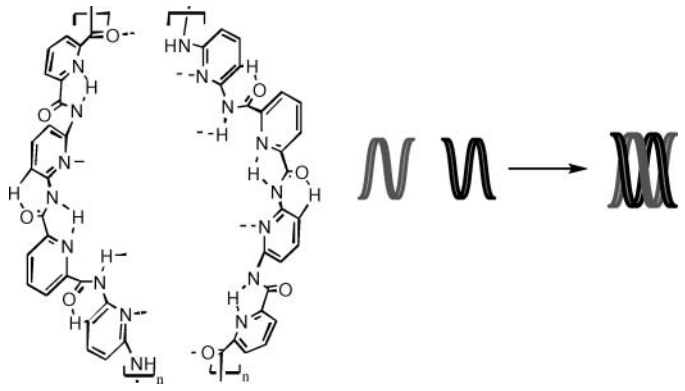

Fig. 2. Intramolecular hydrogen bonds in helical conformations of pyridine-containing polymers and schematic representation of double helix made by interactions of two helical monomers (16).

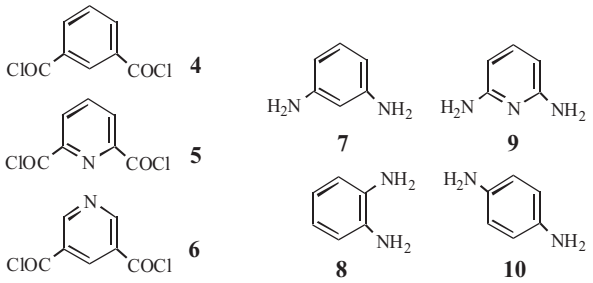

Fig. 3. Monomers used in the polycondensation process.

pyridine in nanoscale using the precipitation polymerization method (25). Incorporation of a transition metal to these polymers group is also studied with the aim of obtaining thermally stable nano-sized polyamides-copper (II) complexes.

2 Experimental

2.1 Materials

Isophthaloyl dichloride **4**, pyridine-2,6-dicarbonyl dichloride **5** and pyridine-3,5-dicarbonyl dichloride **6**, (Fig. 3), were made from the commercial isophthalic acid (Merck), pyridine-2,6-dicarboxylic acid (Aldrich), pyridine-3,5-dicarboxylic acid (Aldrich), respectively, following the literature procedures (26). The commercial diamines **7–10**, hydrated cupric acetate and the solvents 1,4-dioxane (Aldrich) and dimethylsulfoxide (DMSO) (Aldrich) were used as purchased without purification.

2.2 Measurements

Infrared spectra (IR, KBr pellets; 3 mm thickness) were recorded on a Perkin-Elmer Infrared Spectrophotometer (FTIR 1650). All spectra were recorded within the wave number range of 4000–600 cm^{-1} at 25°C. Absorption spectra were measured with a UV 500 UV—Vis spectrometer at room temperature (rt) in DMSO with a polymer concentration of 2 mg/10 mL. ESR measurements of powder samples were recorded at room temperature at the micro-analytical unit, Cairo university using x-band microwave frequency as the first derivative on a Bruker spectrometer utilizing 100 kHz magnetic field modulation with diphenyl picryl hydrazyl (DPPH) as reference material. Differential thermo gravimetric (DTG) analyses were carried out in the temperature range from 13°C to 700°C in a steam of nitrogen atmosphere by a Shimadzu DTG 60H thermal analyzer. The experimental conditions were: platinum crucible, nitrogen atmosphere with a 30 ml/min flow rate and a heating rate 10°C/min. Differential scanning calorimetry (DSC-TGA) analyses were carried out using SDT-Q600-V20.5-Build-15 at the Institute of Graduate Studies

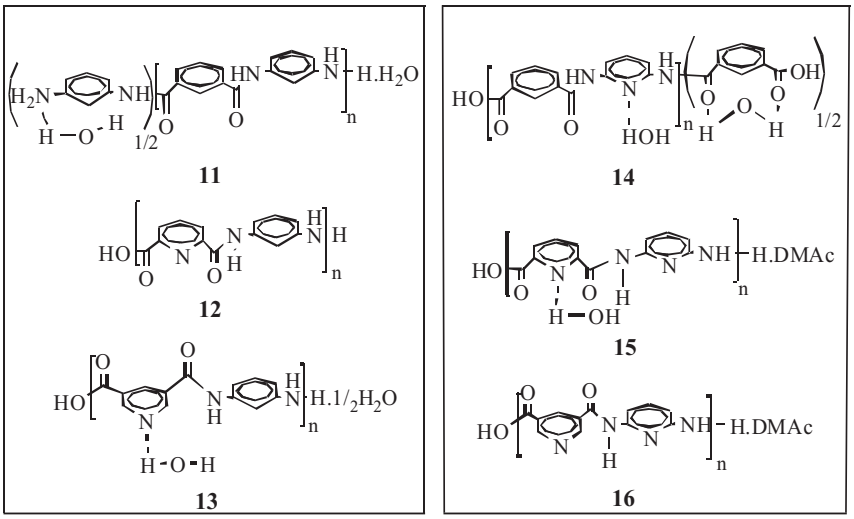

Fig. 4. Chemical Structures of the prepared aramides **11**–**16**.

and Research, Alexandria University. Dielectric measurements were carried out in the frequency range from 0.1 to 5000 kHz using a Hioki 3532 LCR tester, at different temperatures ranging from room temperature up to about 90°C. The polymer powder were pressed to form discs of diameter 10 mm and thickness 1 mm. Silver electrodes were deposited on both sides of the sample surface by thermal evaporation and two copper wires were fixed on the sample using conducting silver paint. Inherent viscosities (η_{inh}) were measured at a concentration of 0.5g/dL in conc. H_2SO_4 at 30°C by using an Ubbelohde viscometer. Elemental analyses were performed at the Microanalytical Unit, Cairo University. The morphologies of polymer nanoparticles were observed by Scanning Electron Microscope (SEM) (JEOL-JSM5300), at the E-Microscope Unit; Faculty of Science, Alexandria University. The samples were sonicated in de-ionized water for 5 min and deposited onto carbon-coated copper mesh and allowed to air-dry before examination.

2.3 Polymer Particles Synthesis (General Method)

The diacid chloride (**4**–**6**) (0.5 mmol) and diamine **7**–**10** (0.5 mmol) were each dissolved in 50 ml dioxane. Distilled water (5 ml) was added to the solution of the diamine followed by addition of the entire acid chloride solution at once. The resulting turbid solution was ultrasonicated at 42 KHz in a water bath for a period of 30 min. The polymer colloidal solution was extracted by centrifugal separation for 15 min at 15000 rpm and the resulting precipitate (∼ 40% yields) was carefully washed with methanol and water to purify the product of any unreacted monomer. The polymer samples were then dried at 100°C for 10 h then kept in a vacuum desiccator.

2.4 Preparation of Cu (II) Complexes Cu11−Cu16 (General Method)

To a stirred suspension of (0.10 mol) of the polyamide in 25 ml DMSO, $Cu(OAc)_2.H_2O$ (0.12 mol) was added. The mixture was vigorously stirred at 90°C for 1 h, then poured while hot on a large amount of crushed ice/H_2O. The dark colored precipitate was filtered, washed with hot methanol and water and dried at 100°C for 10 h then kept in a vacuum desiccator.

3 Results and Discussion

3.1 Synthesis of Symmetrical Wholly Meta-aramides Nanoparticles

Three aromatic acids chlorides (Fig. 3), namely isophthaloyl dichloride **4** pyridine-2,6-dicarbonyl dichloride **5** and pyridine-3,5-dicarbonyl dichloride **6** were used in this investigation. These compounds were prepared by reactions of their corresponding dicarboxylic acids with thionyl chloride in the presence of few droplets of DMF (26). The polyamides nanoparticles **11**–**16** (Fig. 4) were prepared by ultrasonicate 0.5 mmol of *m*-phenylenediamine **7**, 2,6-diaminopyridine **8** with 0.5 mmol of the acid chloride **4**–**6** in a total of 100 ml dioxane solution containing 5 ml water (i.e., 50 ml diamine solution and 50 ml acid chloride solution). SEM photographs of the products **11**–**14** and **15**–**17** are shown in Figures 5, 6, respectively. The polymer structures were confirmed by elemental analysis and IR spectroscopy. Table 1 compiles physical properties of the prepared polymers.

In general, the products **11**–**14** and **16**, Figures 5, 6 prepared in such solution containing water were well-separated spherical particles with some interconnection degree while

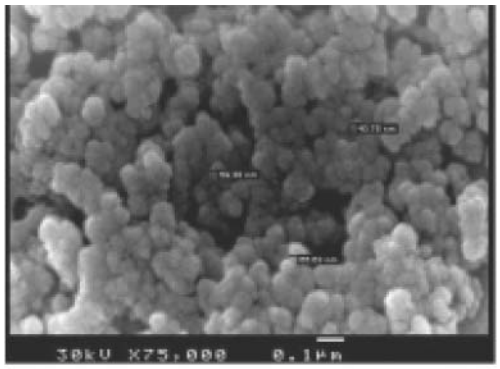

11

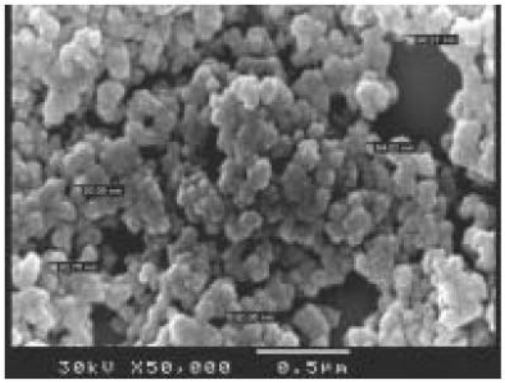

12

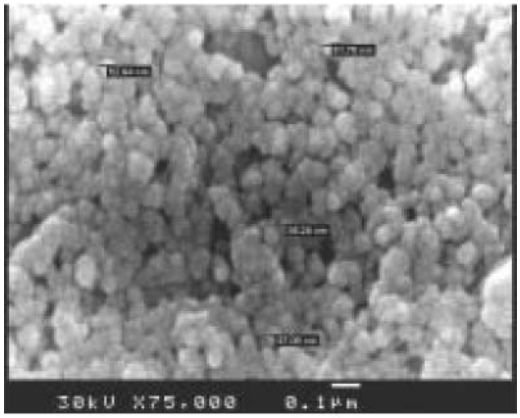

13

Fig. 5. SEM images of polymers **11**–**13**, respectively**,** prepared in 1,4-dioxane/water (100:5 v/v).

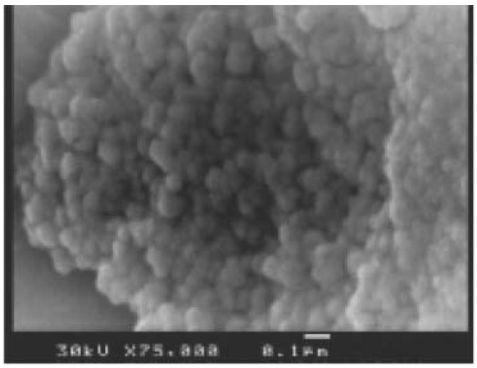

14

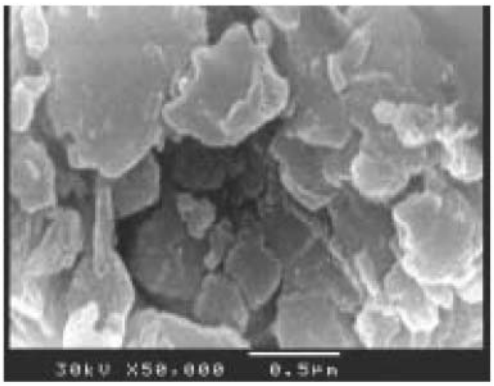

15

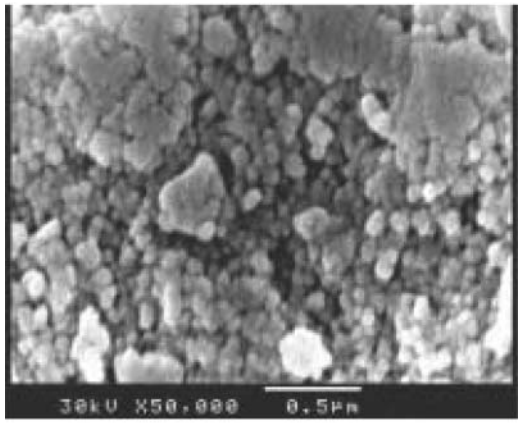

16

Fig. 6. SEM images of polymers **14**–**16,** respectively**,** prepared in 1,4-dioxane/water (100:5 v/v).

polymer **15** was not obtained in a particular form (Fig. 6). Noteworthy, the presence of excess of water content in the reaction (e.g. Dioxane/water 100:10 v/v) was avoided because water hydrolyzes the acid chloride to its corresponding carboxylic acid and thus inhibits the condensation reaction. The average diameter of particles were estimated from SEM images and selected at random. The average diameter of the particles ranges from 50–98 nm. Noteworthy, particles of pyridine containing polymers exhibited large diameter compared to their phenylene counterpart and this result could be attributed to their tendency to form a relatively higher number of H-bonding interactions.

3.2 Physical Properties of the Prepared Polymers

3.2.1. *Solubility*

The prepared pyridine-containing polymers **11**–**16** showed different solubility behaviors in different organic solvents. Moderate to complete dissolutions (5 wt% solid content)

Table 1. Yield (%), elemental analyses, inherent viscosity and IR data of the polymers **11**–**16**

#	*Yield (%)*	*Unit Formula*	*M.Wt*	*% C (Found)*	*% H (Found)*	*% N (Found)*	η_{inh}†	*IR (KBr) (υ cm^{-1})*
11	43	$C_{17}H_{17}N_3O_3.{}^1/_2H_2O$	320	63.75 (63.99)	5.62 (9.69)	13.12 (12.84)	0.898	3297, 3067, 1654 1608, 1540, 1486.
12	40	$C_{13}H_{11}N_3O_3$	257	60.70 (60.58)	4.31 (6.51)	16.33 (16.09)	0.844	3255, 3067, 1674, 1608, 1538, 1489.
13	41	$C_{13}H_{13}N_3O_4.{}^1/_2H_2O$	284	54.92 (54.43)	4.92 (6.73)	14.78 (14.69)	0.870	3279, 3070, 1659, 1609, 1544, 1489.
14	46	$C_{17}H_{16}N_3O_6$	358	56.98 (56.21)	4.46 (5.63)	11.73 (12.43)	0.879	3082, 1689, 1609, 1578, 1542, 1419.
15	44	$C_{16}H_{21}N_5O_5$	363	52.89 (52.77)	5.83 (6.41)	19.27 (19.03)	0.829	3337, 3184, 1702, 1659, 1586, 1456.
16	42	$C_{16}H_{21}N_5O_5$	363	52.89 (52.73)	5.83 (6.00)	19.27 (19.17)	0.850	3337, 3089, 1658, 1604, 1464, 1423.

†The inherent viscosity of the polymers was measured at a concentration of 0.5 g/dL in conc. H_2SO_4 at 30°C.

were observed in a variety of hot aprotic solvents such as NMP, DMSO, DMAc and in hot conc. H_2SO_4 while insoluble in boiling alcoholic solvents such as methanol, ethanol, propanol and ethylene glycol or in halogenated solvents such as $CHCl_3$, CCl_4, CH_2Cl_2, $ClCH_2CH_2Cl$ or in ethers such as Et_2O, THF, 1,4-dioxane or 1,2-dimethoxyethane (DME).

3.2.2. *Inherent Viscosity*

The inherent viscosity of the polymers, as a suitable criterion for evaluation of molecular weight, was measured at a concentration of 0.5 g/dL in H_2SO_4 at 30°C. It was in the range of 0.829–0.898 dL/g that showed moderate molecular weights (Table 1). Thus, it is concluded that the prepared linear symmetric meta-polymers showed high η_{inh} values and thus high degree of polymerization.

3.2.3. *FTIR Spectroscopy*

The FT-IR spectra of the polyesteramides exhibited characteristic absorption bands at around 3300 and 1650 cm^{-1} corresponding to the N-H and C=O stretching of amide group, respectively, while bands at around υ 3050 and 1600 cm^{-1} are due to the aromatic H-C_{str} and C-C_{str}, respectively. Table 1 compiles selected IR bands of the prepared polymers **11**–**16**.

3.2.4. *Optical Properties*

The optical properties of representative polymers were investigated by UV-Vis spectroscopy in DMSO with a polymer concentration of $\sim$ 2 mg/10 mL. Comparison between polyamides derived from different diacid chlorides with the same diamine clearly revealed that the absorption characteristics of the polymer are affected by the linear conjugated system. For instance, polyamides **11**, **12**, **13** exhibited maximum absorption (λ_{max}) at 361, 351 and 311 nm, respectively, due to the $\pi - \pi^*$ transition. It is obvious that the absorption bands of polymer derived from 2,6-pyridine dicarboxylic acid **12** (λ_{max} 351 nm) exhibits a slight red-shift than those derived from 3,5- analogue **13** (λ_{max} 311 nm). Similar observations were noticed in studying the absorption spectra of the polyamides **14, 15**, **16** that showed λ_{max} at 343, 318 and 314 nm, respectively. All of these absorption bands are due to the $\pi - \pi^*$ transitions.

3.2.5. *Thermal Properties*

The thermal properties of the prepared polymers were evaluated by differential thermo gravimetric (DTG), differential thermal analysis (DTA) and differential scanning calorimetry (DSC) techniques. Thermal data of the prepared polymes are complied in Table 2 and their postulated thermal degradation analyses are shown in Figure 7. Thermal results revealed that the prepared polymers have high thermal stability. Structure-thermal property correlation based on changing the dicarboxylic acid monomer, as a single structural modification while the diamine is fixed, demonstrated an interesting connection between a single change and thermal properties. Interestingly, inverting the comparison method, i.e. structural modification in the diamine monomer, is also important to be considered. Polyamides **11, 12** and **13** exhibited three endothermic decomposition peaks at 272°C, 239°C and 303°C, respectively, that clearly demonstrated the high thermal stability of **13** relative to its analogues. Furthermore, **13** showed a higher exothermic thermal degradation peak at 385°C than **12** (300°C, 360°C) and **11** (317°C, 375°C). Thermal analysis data demonstrated that **11** and **12** exhibited similar major decomposition process leaving 72% and 81% of the polymers as remaining mass residues. Polyamides **14**, **15**, **16** obtained showed three endothermic decompositions weight loses peaks at 293, 232°C and 293°C and other three exothermic decompositions peaks at 450°C, 386°C and 360°C, respectively. Interestingly, thermal analyses data of this series demonstrated similar major amide linkage degradation and that **14** exhibited the highest thermal stability. From the data in hand, it can be concluded that products with the same chemical structure showed almost the same degree of thermal stability above a certain molecular weight. The T_d value of phenylene-containing polymers **11** at 28% weight loss was 400°C which is comparable as those of high molecular-weight polymeric fiber of this chemical structure, which is mainly composed of amide bond and benzene ring. Interestingly, *m*-pyridine-containing polymers **12**, **13** also exhibited high thermal stability and thus high molecular weights.

The thermodynamic parameters of decomposition processes of the prepared polymers, namely, activation energy (E_a), enthalpy (ΔH^*), entropy (ΔS^*), and Gibbs

Table 2. Thermoanalytical and the kinetic parameters of the prepared polymers **11**–**16**

#		*TG (°C)*	*% Wt loss Calc.(Found)*	*Fragment* [b]	T^c	$E_a^{\dagger}$	$A(S^{-1})$	$\Delta H^{*\dagger}$	$\Delta S^{*\dagger}$	$\Delta G^{*\dagger}$
11	I	60–190	5.62 (5.93)	H_2O	336	15.95	0.00391	13.16	–0.29	111.24
	II	200–375	28.28 (28.11)	$(C_6H_9N_2O)_{1/2}.CO$	545	38.29	21726.5	33.76	–0.17	124.77
	III	380–700	71.56 (71.89)[a]	$C_{13}H_{13}N_2O_2$	591	19.15	4852438055	14.24	–0.05	41.43
					649	38.29	0.00274	32.90	–0.30	227.86
12	I	65–120	6.61 (5.36)	NH_3	338	9.57	5431.67	6.76	–0.17	65.71
	II	239–360	13.22 (13.75)	$2H_2O$	512	3.83	0.00054	−0.43	–0.31	159.43
	III	360–700	80.93 (80.88)[a]	$C_{13}H_8N_2O$	634	3.06	0.00024	−2.21	–0.32	201.05
13	I	69–166	6.33 (6.67)	H_2O	338	14.36	0.00480	11.54	–0.29	109.78
	II	190–385	14.78 (13.39)	$NH_2OH.1/2H_2O$	440	12.76	0.00144	9.12	–0.30	142.15
	III	385–700	78.87 (79.46)[a]	$C_{13}H_8N_2O_2$	575	19.15	0.00227	14.36	–0.30	187.49
					659	6.38	0.00068	0.90	–0.31	206.49
14	I	50–175	2.51 (3.29)	$1/2H_2O$						
	II	200–450	39.38 (39.95)	$C_8H_4O_2.1/2H_2O$	565	38.29	0.07638	33.59	–0.27	187.13
	III	450–700	55.72 (56.33)[a]	$C_9H_{10}N_3O_3$						
15	I	51–178	5.15 (4.95)	H_2O	335	22.98	0.00927	20.19	–0.28	115.73
	II	232–386	45.45 (43.76)	$C_7H_5N_2O_3$	504	19.15	0.00924	14.96	–0.29	160.22
	III	390–700	49.58 (50.35)[a]	$C_9H_{14}N_3O$	660	63.82	0.00334	58.34	–0.30	255.56
16	I	51–175	2.57 (2.81)	$1/2H_2O$						
	II	232–386	45.45 (43.76)	$C_7H_5N_2O_3$	564	38.29	0.05984	33.60	–0.27	187.96
	III	386–700	49.58 (50.35)[a]	$C_9H_{14}N_3O$						

[a]% Residue.
[b]Structural formulas for all fragments are given in Figure 7.
[c]The peak temperature from the DTG charts.
[†]Values are in kj/mole.

free energy change of (ΔG^*) were evaluated graphically by employing the Coats-Redfern method (27, 28). The kinetic data obtained from the nonisothermal decomposition of the prepared polymers are given in Table 2. Activation energies values (E_a) of polyamide series (**14**, **15**, **16**) demonstrated that **14** and **16** have identical E_a which is nearly one half of E_a **15**. According to the kinetic data obtained from DTG curves, all polymers have negative entropy (ΔS^*), which indicates ordered systems and more ordered activated states that may be possible through the chemosorption of other light decomposition products.

3.3 Synthesis of Unsymmetrical Aramides Nanoparticles

One important task in our study is to analyze and predict the detailed polymer structure that could increase the

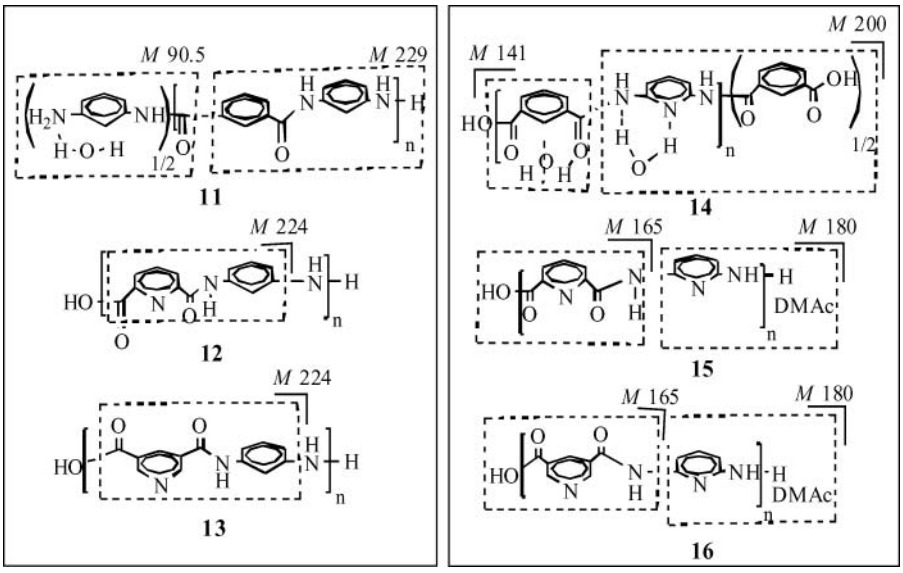

Fig. 7. Thermal degradation analysis of the investigated polyamides **11**–**16**.

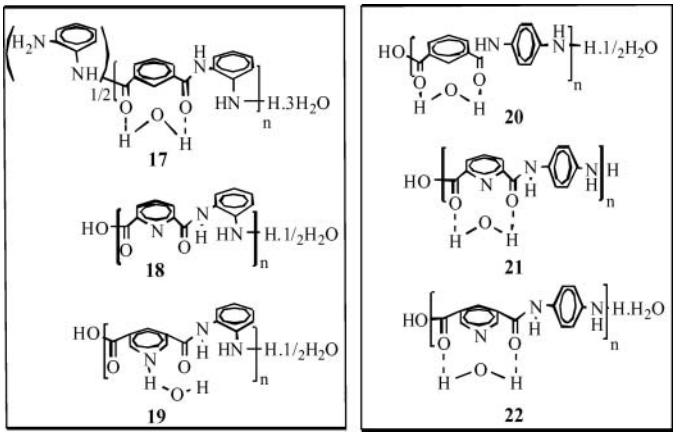

Fig. 8. Chemical Structures of the prepared aramides **17**–**22**.

thermal stability, which directly affect processing and practical application. It is interesting to correlate the structure-property relationship, in particular, studying the influence of the linear conjugation on the polymer properties. Thus, and for comparison reasons, the synthesis of polymers **17**–**22** was considered. The aramides nanoparticles **17**–**19** and **20**–**22**, (Fig. 8) were respectively prepared by ultrasonicate 0.5 mmol of *o*-phenylenediamine **9** and *p*-phenylenediamine **10** with 0.5 mmol of the acid chloride **4**–**6** in a total of 100 ml dioxane solution containing 5 ml water. The polymer structures were confirmed by elemental analysis and IR spectroscopy. Table 3 compiles physical properties of the prepared polymers.

Aramides **17**–**22** exhibited similar physical properties as their analogues **11**–**16**, nevertheless, the latter linear wholly meta-polymers showed relatively higher η_{inh} values and thus higher degree of polymerization than the former polymers derived from non-symmetric analogues.

The absorption spectra of the polyamides **17–19** and **20–22** are shown in Figure 9, respectively. Comparison between polyamides derived from different diacid chlorides with the same diamine clearly revealed that the absorption characteristics of the polymer are affected by the linear conjugated system. It is obvious that the absorption bands of polymer derived from 2,6-pyridine dicarboxylic acid **21** (λ_{max} 323 nm) exhibit a slight red-shift than those derived from 3,5-analogue **22** (λ_{max} 319 nm) and **20** (λ_{max} 314 nm). Similar observations were noticed in studying the absorption spectra of the polyamides **17, 18**, **19** showed λ_{max} at 282, 302 and 292 nm, respectively. All of these absorption bands are due to the $\pi - \pi^*$ transitions.

Thermal and kinetic data of polymers **17**–**22** are compiled in Table 4 and their postulated thermal degradation analyses are shown in Figure 10.

Polyamides **20, 21**, **22** derived from *p*-phenylenediamine **10** and polyamides **17, 18**, **19** derived from *o*-phenylenediamine **9** exhibited a similar thermal behavior. Previous reports have shown that T_d remains constant for products of high molecular weight above a certain level (29). Polyamides **17**, **18**, **19** obtained from **9** showed three endothermic decompositions weight loses peaks at 293, 232°C and 293°C and other three exothermic decompositions peaks at 450°C, 386°C and 360°C, respectively. Interestingly, thermal analyses data of this series demonstrated similar major amide linkage degradation and that **17** exhibited the highest thermal stability.

3.4 Preparation of Polyamides-copper (II) Complexes

Polyamides **11**–**16** took the center stage with the performance as these symmetrical materials exhibited higher thermal stability and thus higher molecular weights than other analogues and their properties can be tuned as semiconducting nanoparticles for many industrial applications. Incorporation of a transition metal to these polymers group was our next goal. The complexation reaction was carried out by careful addition of $Cu(OAc)_2.H_2O$ (1.2 equivalent)

Table 3. Yield (%), elemental analyses, inherent viscosity and IR data of polymers **17**–**22**

#	*Yield (%)*	*Unit Formula*	*M.Wt*	*% C (Found)*	*% H (Found)*	*% N (Found)*	η_{inh}†	*IR (KBr) (υ cm^{-1})*
17	44	$C_{17}H_{15}N_4O_2.4H_2O$	379	53.82 (53.66)	6.06 (7.55)	14.77 (13.86)	0.763	3235, 3065, 1650, 1599, 1522, 1489.
18	44	$C_{13}H_{11}N_3O_3.{}^1/_2H_2O$	266	58.64 (58.97)	4.51 (6.43)	15.78 (16.30)	0.712	3242, 3086, 1700, 1683, 1595, 1529.
19	42	$C_{13}H_{13}N_3O_4.{}^1/_2H_2O$	284	54.92 (54.98)	4.92 (7.02)	14.78 (15.05)	0.750	3693–2855, 1705, 1659, 1601, 1528.
20	40	$C_{14}H_{13}N_2O_4.{}^1/_2H_2O$	282	59.57 (59.56)	4.96 (6.16)	9.92 (8.68)	0.790	3287, 3060, 1698, 1644, 1609, 1580.
21	42	$C_{13}H_{13}N_3O_4$	275	56.72 (55.91)	4.76 (7.72)	15.27 (15.81)	0.745	3258, 3055, 1658, 1606, 1447, 1513.
22	42	$C_{13}H_{15}N_3O_5$	293	53.24 (53.66)	5.16 (7.55)	14.33 (15.36)	0.760	3278, 3058, 1704 1658, 1561, 1513.

†The inherent viscosity of the polymers was measured at a concentration of 0.5g/dL in conc. H_2SO_4 at 30°C.

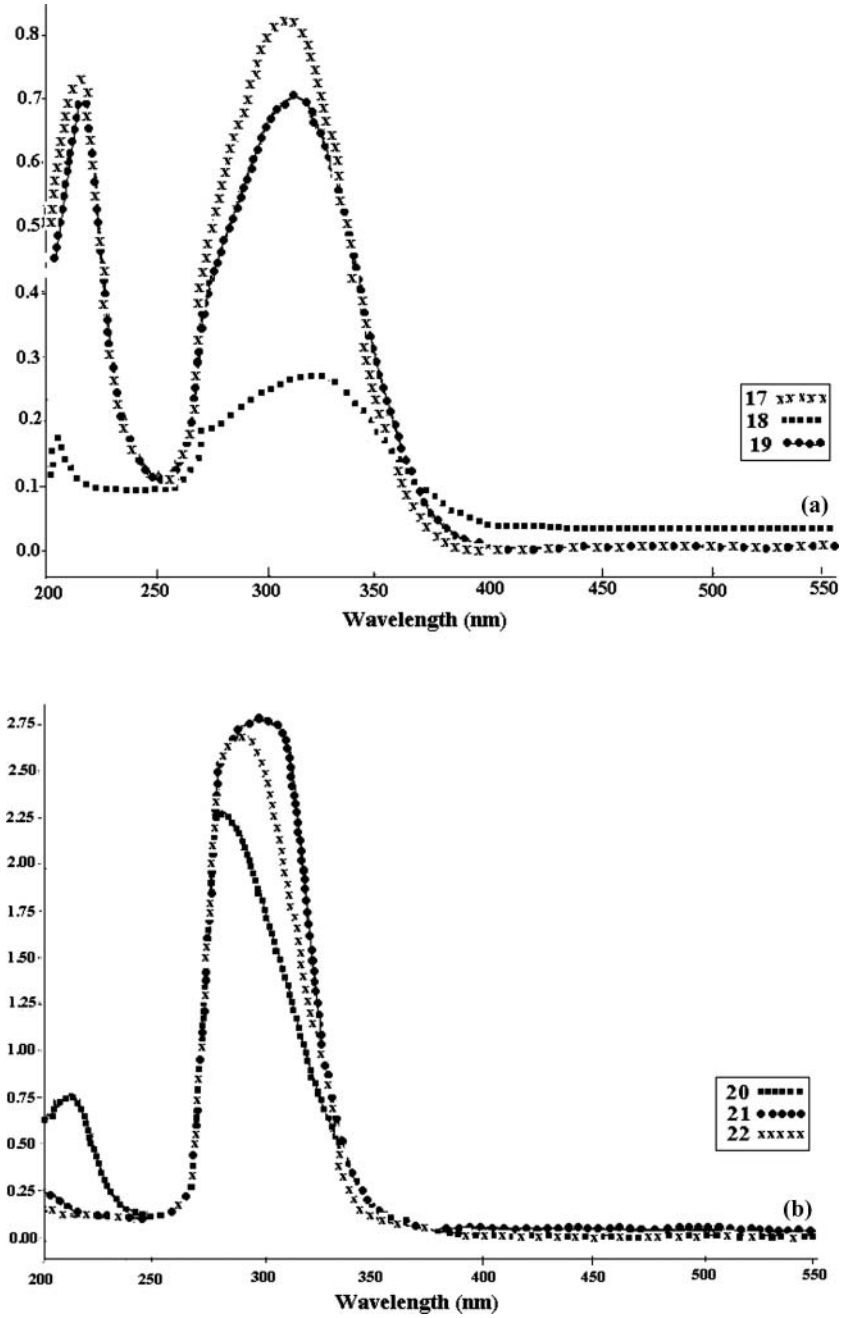

Fig. 9. Absorption spectra of polyamides: (a) **17–19** and (b) **20**–**22**.

to the stirred hot solution of the polymer in DMSO at (80–90°C) for 1h. The Cu (II) ions were complexed with polymer repeating unit in a ratio of 1:2 and the complexes structures **Cu11**−**Cu16** given in Figure 11 are proposed on the basis of their spectral and elemental analyses data (Table 5). Pyridine-containing polymers **Cu12**, **Cu13** showed similar sites of metal coordination and hence the metal ion accommodates inside the inner cavity made by the pyridine nitrogen atom with two hydrogen amide atoms pointing towards the cavity while the carbonyl groups are directed outside of the inner cavity producing five- and six-membered chelate rings, respectively. The appearance of the sharp (Cu−N) bands at υ 678 and υ 680 cm^{-1} in these complexes unambiguously proved that the pyridine nitrogen atom represents the central binding site. Copper complexes **Cu14**–**Cu16** showed bands at *ca* υ1600 cm^{-1} and 1230 cm^{-1} corresponding to C= N and C−NO, respectively, while bands around 600 cm^{-1} are attributed to υ (M-N) (30).

The electronic spectra of the complexes **Cu11**–**Cu16** were investigated by UV-Vis spectroscopy in DMSO with

Table 4. Thermoanalytical and the kinetic parameters of the prepared polymers **17**–**22**

#		*TG (°C)*	*% Wt. loss Calc.(Found)*	*Fragment* [b]	T^c	$E_a^{\dagger}$	$A(S^{-1})$	$\Delta H^{*\dagger}$	$\Delta S^{*\dagger}$	$\Delta G^{*\dagger}$
17	I	80–160	4.74 (4.05)	H_2O	378	19.14	0.00320597	16.00	–0.29	127.31
	II	200–378	72.29 (72.65)	$C_{14}H_{14}N_2O_4$	563	30.08	0.00887666	25.40	–0.29	188.41
	III	384–700	21.24 (22.92)[a]	$C_6H_9N_2O.H_2O$	656	38.29	0.02123195	32.84	–0.28	218.80
18	I	52–213	6.76 (6.4)	H_2O	342	10.64	4883048074	7.79	–0.06	28.52
	II	287–376	76.31 (76.25)	$C_{10}H_9N_3O_2$	558	22.97	0.03413	18.34	–0.28	173.55
	III	380–700	16.91(17.35)[a]	CHO_2	650	67.01	0.065468	61.61	–0.27	239.85
19	I	74–190	6.33 (5.83)	H_2O	348	1.87	0.00263449	−1.01	–0.30	101.74
	II	200–345	71.47 (71.42)	$C_{10}H_9N_3O_2$	463	23.93	0.02055275	20.08	–0.28	150.22
	III	350–700	22.53 (22.78)[a]	HCOOH, -H_2O	610	47.86	0.15271436	42.79	–0.27	205.56
20	I	71–190	3.19 (2.45)	$^1/_2H_2O$	344	14.55	0.0168566	11.69	–0.30	114.75
	II	200–371	28.01 (27.00)	CO_2, NH_4OH	421	15.31	0.00115093	11.81	–0.30	139.97
	III	371–700	69.14 (70.55)[a]	$C_{13}H_9NO$	520	22.97	0.00486564	18.65	–0.29	171.54
					604	19.15	0.00202283	14.12	–0.30	196.92
					645	19.15	9681886787	13.78	–0.04	40.23
21	I	62–191	3.27 (3.41)	$^1/_2H_2O$	335	3.00	2259435770	0.22	–0.07	22.62
	II	252–381	20.00 (18.60)	HCOOH. $^1/_2H_2O$	465	0.48	0.000131	−3.39	–0.32	146.79
	III	381–700	77.09 (77.99)[a]	$C_{12}H_{10}N_3O$	525	5.74	0.001306	1.38	–0.30	161.52
					604	19.14	10863.255	14.13	–0.17	118.89
					655	19.15	0.002023	13.70	–0.30	212.15
22	I	49–192	3.07 (3.38)	$^1/_2H_2O$	322	9.57	0.00384529	6.89	–0.29	100.95
	II	257–363	18.77 (19.76)	HCOOH. $^1/_2H_2O$	400	1.47	0.00049513	−1.85	–0.31	122.46
	III	363–700	78.49 (77.11)[a]	$C_{12}H_{10}N_3O.H_2O$	466	5.47	8051652074	1.60	–0.06	29.06
					539	7.05	0.00138771	2.57	–0.30	166.82
					620	1.53	614964435	−3.62	–0.08	47.69

[a]% Residue.
[b]Structural formulas for all fragments are given in Fig. 10.
[c]The peak temperature from the DTG charts.
†Values are in kj/mole.

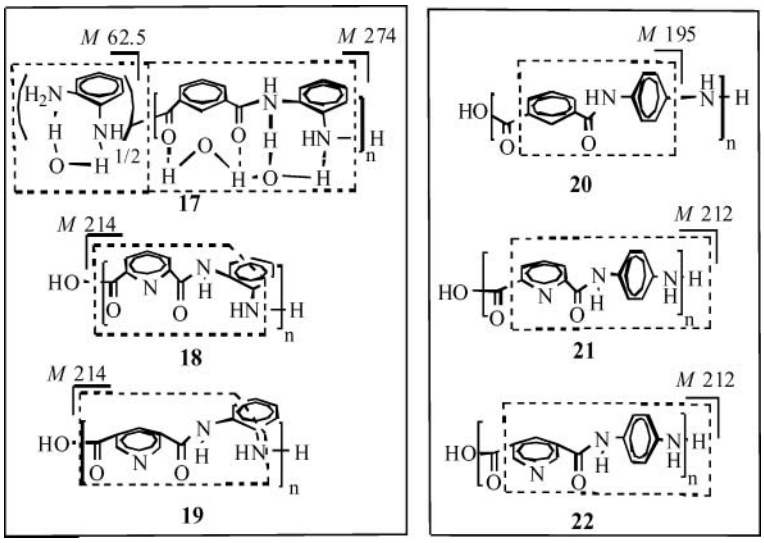

Fig. 10. Thermal degradation analysis of the investigated polyamides **17**–**22**.

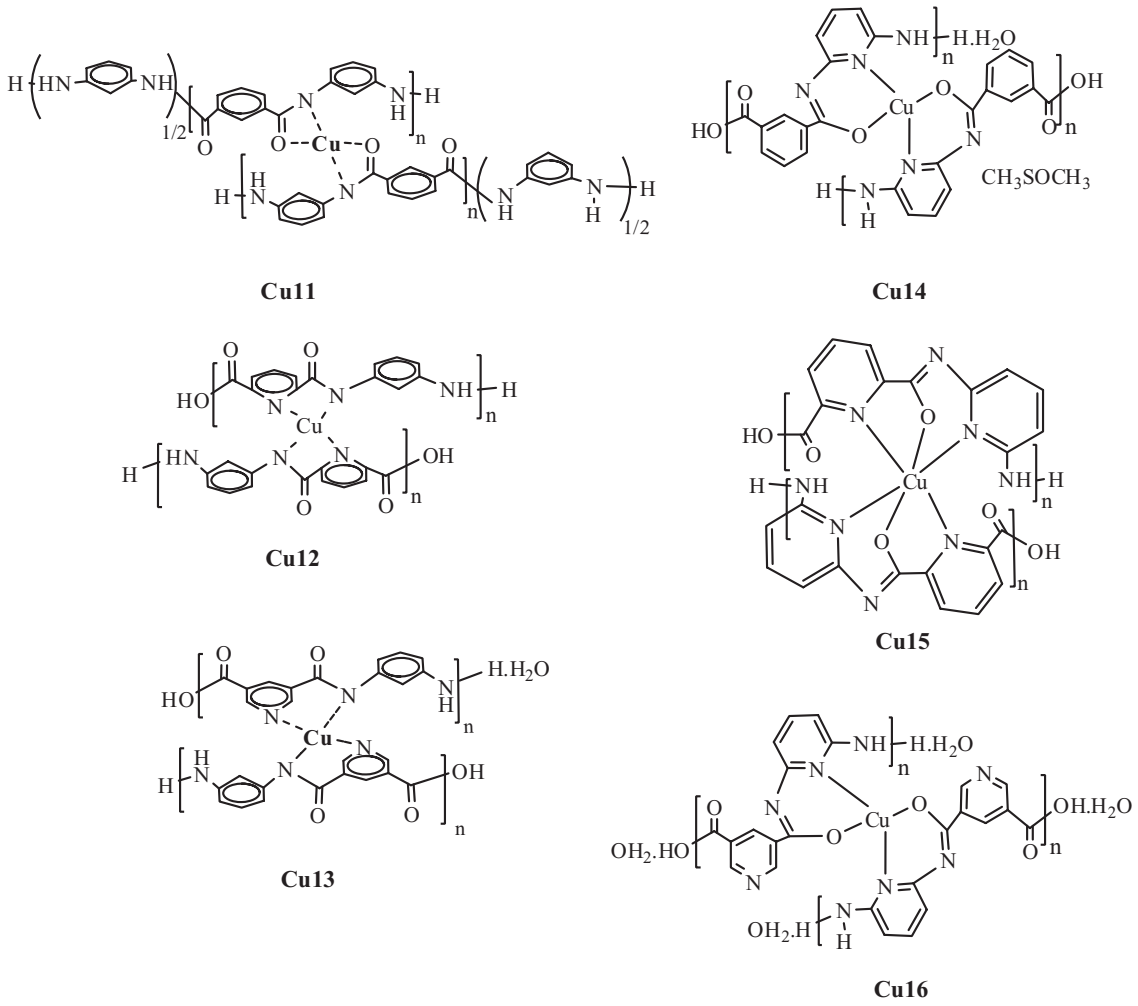

Fig. 11. Proposed chemical structures of the prepared complexes **Cu11**–**Cu16**.

polymers concentrations of 10^{-3} M, (Fig. 12) and the maximum absorptions (λ_{max}) and absorption values (A) are compiled in Table 5. The electronic spectra of the complexes showed bands at 427 nm, 420 nm, 396 nm, 394 nm, 425 nm and 402 for **Cu11**–**Cu16**, respectively, which are attributed to the ligand-metal charge transfer (LMCT) transitions from the conjugated *n*- and *p*-orbitals of the donor to d orbitals of the metal. In addition, **Cu12** exhibited a shoulder at λ_{max} 610 while **Cu15** showed a highly red shifted band at λ_{max} 901 and both of these bands are due to the expected d-d transition (31).

The complexation of polymers **11**–**16** with hydrated $Cu(OAc)_2$ produce charge-transfer complexes which would give an effective contribution to the optical properties of the polymer. The charge carriers in complexes **Cu12**, **Cu13** and **Cu14**, **Cu16** are generated by activation of the *n*-electrons of the pyridine N-atom after doping with Cu $(OAc)_2.H_2O$. In these polymers, the Cu^{+2} ion accommodates inside the inner cavity made by the pyridine nitrogen atom with the two surrounding amide nitrogen atoms producing five- and six-membered chelate rings, respectively. In case of **Cu15**, the Cu^{+2} ion formed two fused five and six membered chelate rings. The five membered ring chelates are thermodynamically more stable than six-membered chelate rings and thus, one might expect a higher mobility ligand-metal-ligand charge transfer in the former chelate ring size than the latter one.

The ERS parameters of copper (II) complexes **Cu11**–**Cu16** are presented in Table 5. The ERS spectra of the copper compounds in the polycrystalline state at room temperature are quite similar and exhibited typical axial spectra with g// and g⊥ features, where the g-tensors obey the criterion $g_{//} > g_{\perp} > 2.0023$. These data indicate that the copper site has a d_{x2-y2} ground state, characteristic of square planar or elongated octahedral stereochemistry (32). As judged by spectral and elemental data, complexes **Cu11–Cu14** and **Cu16** have square planar geometry while **Cu15** has a six coordinate octahedral geometry. In an axial symmetry, g-values are related by the expression $G = (g_{//}-2)/(g_{\perp}-2)$ which measures the exchange interactions

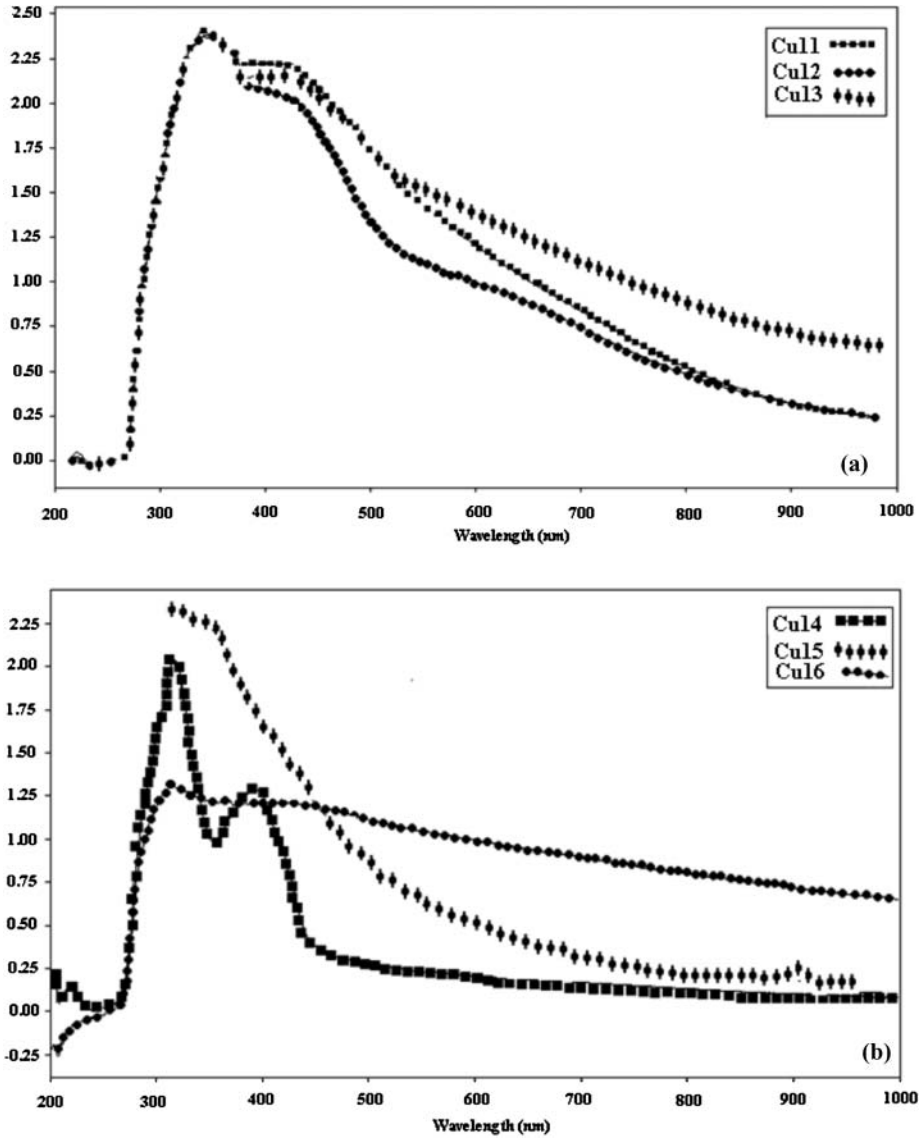

Fig. 12. Absorption spectra of polyamides complexes: (a) **Cu11**–**Cu13**, (b) **Cu14–Cu16**.

between copper centers and polycrystalline solids. The calculated G-values were found less than four suggesting considerable exchange interaction in solid complexes (33).

The thermal properties of the prepared polymers were evaluated by differential thermo gravimetric (DTG), thermogravimetric analysis (TGA) and differential scanning calorimetry (DSC) techniques. Figure 13 shows the TGA curves of the prepared copper complexes **Cu11**–**Cu16** while Figure 14 shows the DSC curves of **Cu14–Cu16**, respectively. Thermal data of the prepared polymers are complied in Table 6 and the results revealed the high thermal stability of polymers **Cu11–Cu16**. Interestingly, thermal analysis data of this series demonstrated similar major amide linkage degradation and polyamides-containing pyridine **Cu12**, **Cu15** exhibited the highest thermal stability. The total mass loss values of this polymers series proved the loss of nearly 40–48% of masses throughout the entire thermal stages up to 700°C and the remaining residues attributed to their corresponding fragments A, (Fig.15) These results further confirm the proposed compositions of the complexes **Cu11**–**Cu16**.

The kinetic data obtained from the nonisothermal decomposition of the prepared copper complexes are given in Table 6. Activation energies values (E_a) of polyamides complexes (**Cu11**–**Cu16**) demonstrated higher E_a values compared to their corresponding free ligands. Noteworthy, complexes **Cu12** and **Cu13** have nearly the same E_a values for the first and second decomposition steps which indicate similar degradation mechanism in both compounds, while the last decomposition step of this series **Cu11**–**Cu13** was in the order **C12**>**Cu13**>**Cu11**. This may be attributed to the ring size effect where **Cu12** has a five membered chelate

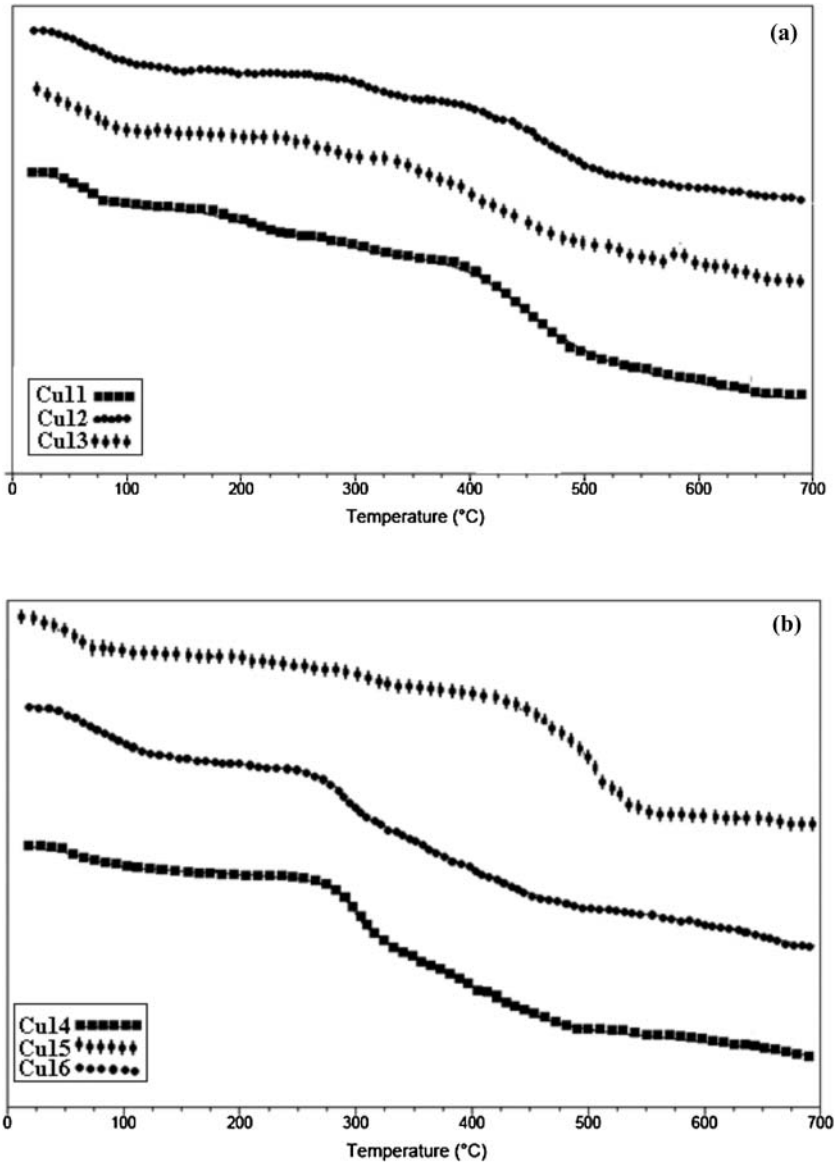

Fig. 13. TGA curves of polymers copper complexes: (a) **Cu11**–**Cu13**, (b) **Cu14**–**Cu16**.

structure which is thermodynamically more stable than the chelate structures of **Cu11** and **Cu13**.

Activation energies of the series **Cu14**–**Cu16** demonstrated that E_a was in the order **Cu15**>**Cu14**>**Cu16** which is attributed to the number of the formed chelate rings. **Cu15** has four chelate rings while **Cu14** and **Cu16** have two chelate rings and thus one might expect a relatively easy thermal degradation process of the latter two compounds compared to the former one. It is interesting to note that the energy of activation reflects the kinetic lability of the complexes. The compounds with lower E_a values are more labile as compared to those with higher E_a values (34). According to the kinetic data obtained from DTG curves all polymers have negative entropy (ΔS^*), which indicates ordered systems and more ordered activated states that may be possible through the chemosorption of other light decomposition products.

Electrical properties of conjugated polymers have been studied for many years (35) because of their attractive electronic and optoelectronic properties. One of the most important goals is to develop narrow-band gap polymers in the field of materials science. Hence, to find low energy gap parent molecules is the key step of designing conductive polymer. Currently, this topic attracted interest in many areas of materials research such as in organic light-emitting displays (LEDs), field-effect transistors (FETs), solar cells and switching devices and so forth. The temperature dependence vs. dc conductivity for the copper complexes **Cu11–Cu16** plotted as σ (Ω^{-1} cm^{-1}) vs. T (K) is presented in Figure 16 and their conductivity values are listed in Table 7.

Table 5. Yield (%), elemental analyses, λ_{max}, absorption values (A) and g-tensors of polymers **Cu11-Cu16**

No.	*Yield (%)*	*Unit Formula*	*M.Wt*	*% C (Exp.)*	*% H (Exp.)*	*% N (Exp.)*	λ_{max} *(A)*	*IR, υ (cm^{-1})*	$g_{\perp}$	$g_{//}$	*Color*
Cu11	85	$(C_{17}H_{16}N_3O_3)_2Cu.H_2O$	701.5	58.16 (58.11)	4.56 (4.28)	11.97 (10.89)	427 (2.18) 362 (2.37) 341 (2.41)	1657, 1604, 1530, 1479, 1411, 1295, 1238, 1238, 1012, 941, 687, 574.	2.07672	2.17882	Dark brawn
Cu12	82	$(C_{13}H_{10}N_3O_3)_2Cu$	575.5	54.21 (54.13)	3.47 (3.81)	14.59 (14.08)	610 (0.97) 420 (2.03) 358 (2.39)	3330, 1671, 1603, 1529, 1017, 783, 742, 677	2.07609	2.1503	Dark brawn
Cu13	88	$(C_{13}H_{10}N_3O_3)_2Cu.\ H_2O$	593.5	52.56 (52.11)	3.70 (3.97)	14.15 (13.59)	396 (2.19) 367 (2.38)	3330, 1665, 1604, 1537, 1482, 1414, 1282, 1126, 1016, 943, 780, 689, 597	2.07644	2.17565	Dark brawn
Cu14	90	$(C_{13}H_{10}N_3O_4)_2Cu.DMSO.{}^1/_2H_2O$	681	49.33 (49.93)	4.25 (4.58)	12.33 (11.73)	394 (1.28) 318 (2.04)	3330, 2996, 1677, 1604, 1531, 1446, 1391, 1298, 1237, 1013, 944, 796, 723.	2.07132	2.16429	Brawn
Cu15	88	$C_{24}H_{26}N_8O_{10}Cu$	650	44.34 (44.35)	4.03 (4.39)	17.24 (17.44)	901 (0.62) 425 (2.15) 366 (2.36) 340 (2.33) 312 (1.50)	3332, 1696, 1608, 1582, 1518, 1451, 1363, 1317, 1243, 1145, 1072, 1002, 946, 840, 790, 726, 672, 603.	2.09469	2.14365	Dark brawn
Cu16	86	$C_{24}H_{30}N_8O_{12}Cu$	686	42.01 (42.61)	4.41 (4.48)	16.33 (16.02)	402 (0.43) 310 (0.55)	3330, 1675, 1588, 1533, 1444, 1376, 1292, 1238, 1120, 1023, 947, 794, 599,	2.1077	2.12354	Dark brawn

Table 6. Thermoanalytical and the kinetic parameters of the prepared polymers **Cu11-Cu16**

#	*TG (°C)*	*Wt Loss (%) Calc (Found)*	*Fragment*	*Residue (%) Calc (Exp.)*	*Fragment (A)*†	*DTG (°C)*	E_a^b	*A* (S^{-1})	ΔH^{*b}	ΔS^{*c}	ΔG^{*b}
						50	9.58	0.00192	6.89	−278.49	96.84
Cu-11	13–150	08.91 (8.84)	$(C_6H_7N_2.H_2O)_{1/2}$	48.78 (48.28)	$C_{15}H_9CuN_3O_3$	200	60.369	0.00107	56.436	−305.60	200.98
	150–275	43.22 (42.79)	$C_{19}H_{17}N_3O$			320	89.86	0.00900	84.93	−213.25	211.41
	275–700					465	37.65	0.378	31.51	−260.57	223.81
Cu-12	13–175	11.12 (11.47)	$HCOOH.H_2O$	52.29 (52.54)	$C_{12}H_6CuN_4O_2$	86	20.05	0.00127	17.06	−301.60	125.66
	250–700	35.09 (35.16)	$(C_6H_6N)_2.H_2O$			320	57.99	0.000231	53.05	−320.29	136.87
						494	72.45	0.00145	66.07	−307.16	301.66
Cu-13	13–135	13.81 (13.03)	$HCO_2H.2H_2O$	45.82 (44.95)	$C_{12}H_6CuN_2O_2$	65	20.915	0.00209	18.09	−239.86	99.16
	175–340	07.75 (7.74)	HCO_2H			275	56.04	0.001844	53.48	−302.33	220.40
	340–700	33.02 (33.15)	$C_{12}H_{10}N_3$			400	43.98	0.00088	38.38	−310.21	247.15
Cu-14	13–185	06.75 (7.35)	HCO_2H	41.74 (41.81)	$C_{12}H_8CuN_4O$	65	16.05	0.01	13.24	−284.14	109.28
	225–700	49.04 (49.66)	$(C_8H_5O_3)_2.2H_2O$			313	136.35	0.0086	131.47	−290.13	301.70
Cu-15	13–175	11.07 (11.46)	$4x\ H_2O$	44.53 (43.02)	$C_{12}H_8CuN_3O_2$	72	19.43	3.89	16.56	−234.85	97.55
	240–400	07.07 (7.08)	HCO_2H			300	58.97	3.73×10^2	54.20	−201.20	169.49
	400–530	35.38 (36.46)	$(C_5H_4N_2)_2.HCO_2H$			522	154.83	19.58×10^5	150.49	−228.36	269.58
Cu-16	13–200	13.11 (12.10)	$5x\ H_2O$	48.87 (49.94)	$C_{12}H_{12}CuN_6O_2$	93	28.64	0.574	25.60	−251.26	117.48
	200–700	35.56 (36.98)	$(C_6H_4NO_2)_2$			302	111.24	0.00705	106.45	−291.61	274.12

†Structural formulas of the remaining residues of polymers **Cu11-Cu16** up to 700°C are given in Figure 15.
[b]Values are in kj/mole.
[c]Values are in jK/mole.

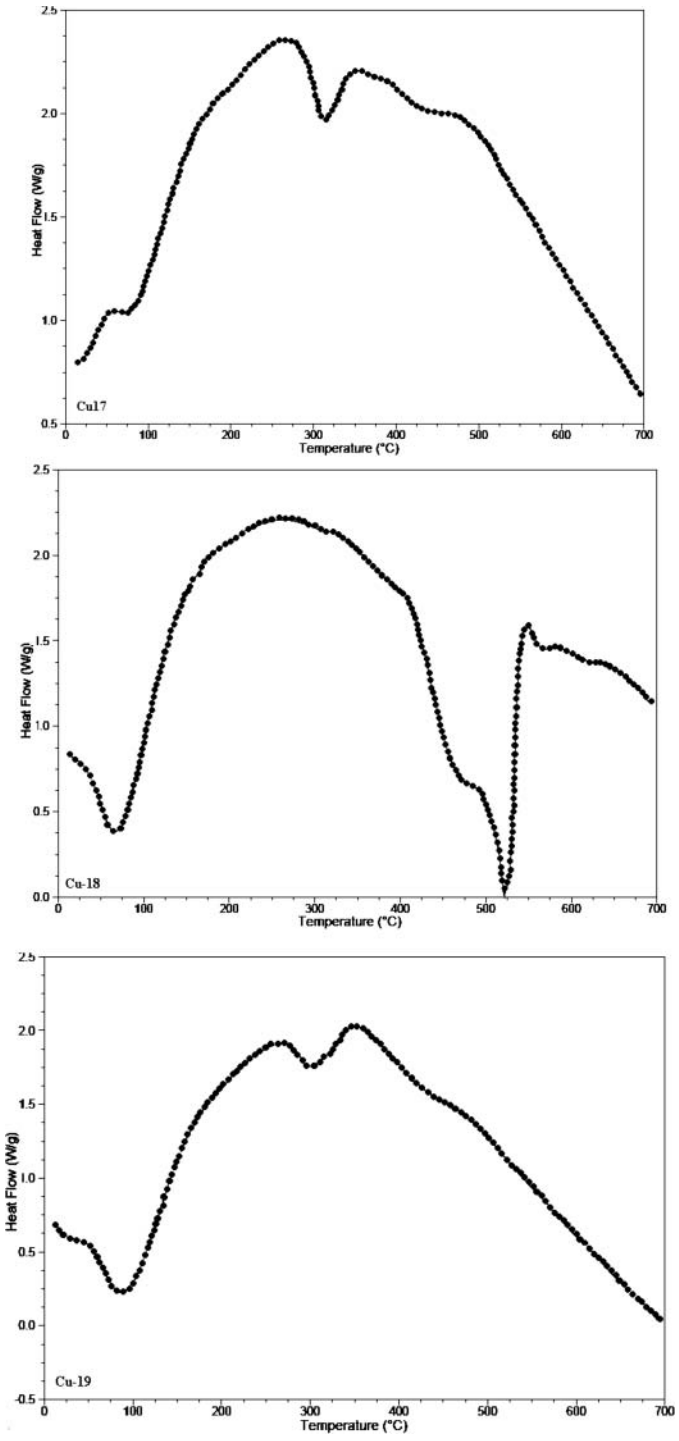

Fig. 14. DSC curves of polymers copper complexes **Cu14** (upper),**Cu15** (middle),**Cu16** (down).

The dc electrical conductivity results of polymers **Cu11–Cu16** revealed different behaviors and it is obvious that the polymer structural variations play a major role in determining the electrical conduction efficiency of the complexes. The conductivity of **Cu11** and **Cu13** did not change with increasing temperature; however, the former exhibited

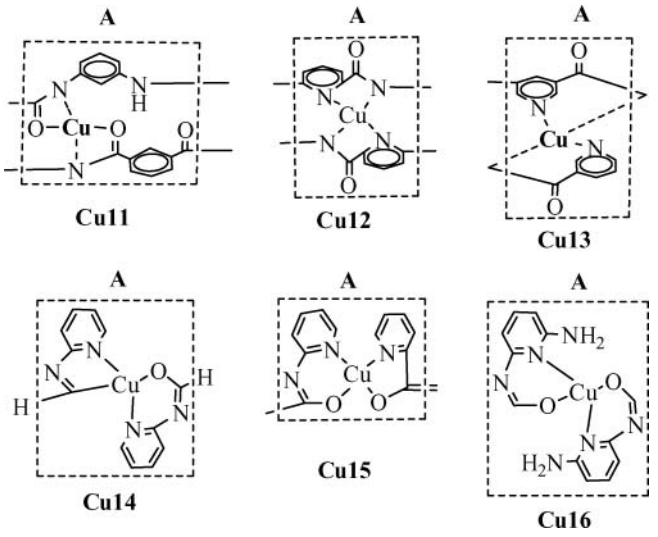

Fig. 15. Structural formulas of the remaining residues of polymers **Cu11**–**Cu16** up to 700°C.

a slight σ improvement compared to the latter. Interestingly, the dc conductivity of pyridine-containing polymer **Cu12** increases with increasing temperature and revealed a double order of magnitude improvement compared to analogues **Cu11** and **Cu13**. This result not only revealed the semi-conducting nature of this specific sample as it obeys the three dimensional Mott variable-range hopping model (36).

In a similar fashion, the conductivity of **Cu14** and **Cu15** did not change with increasing temperature; however, the latter exhibited ten orders of magnitude higher than the former. Interestingly, the dc conductivity of pyridine-containing polymer **Cu16** slightly decreases with increasing temperature and this behavior is indicative of semi-conducting nature in the extrinsic range which is characterized by high carriers and low mobility.

Noteworthy, in the case of **Cu12** and **Cu15** polymers, the Cu^{+2} ion accommodates inside the inner cavity made by the pyridine nitrogen atom with the nitrogen atom of the surrounding amide group producing thermodynamically stable two fused five membered rings chelate and one might expect a higher mobility ligand-metal-ligand charge transfer in such chelate rings. This would explain the higher conductivity of the complexes **Cu12** and**Cu15** compared to other analogues.

Table 7. Electrical conductivity (σ) for polymers **Cu11**–**Cu16** at 290–380 K range in Ω^{-1} cm^{-1}

#	$\sigma\,(\Omega^{-1}\,cm^{-1})$	#	$\sigma\,(\Omega^{-1}\,cm^{-1})$
Cu11	1.27×10^{-7}	**Cu14**	4.56×10^{-9}
Cu12	$1.73-1.82 \times 10^{-7}$	**Cu15**	1.09×10^{-8}
Cu13	1.09×10^{-7}	**Cu16**	$6.73-1.48 \times 10^{-9}$

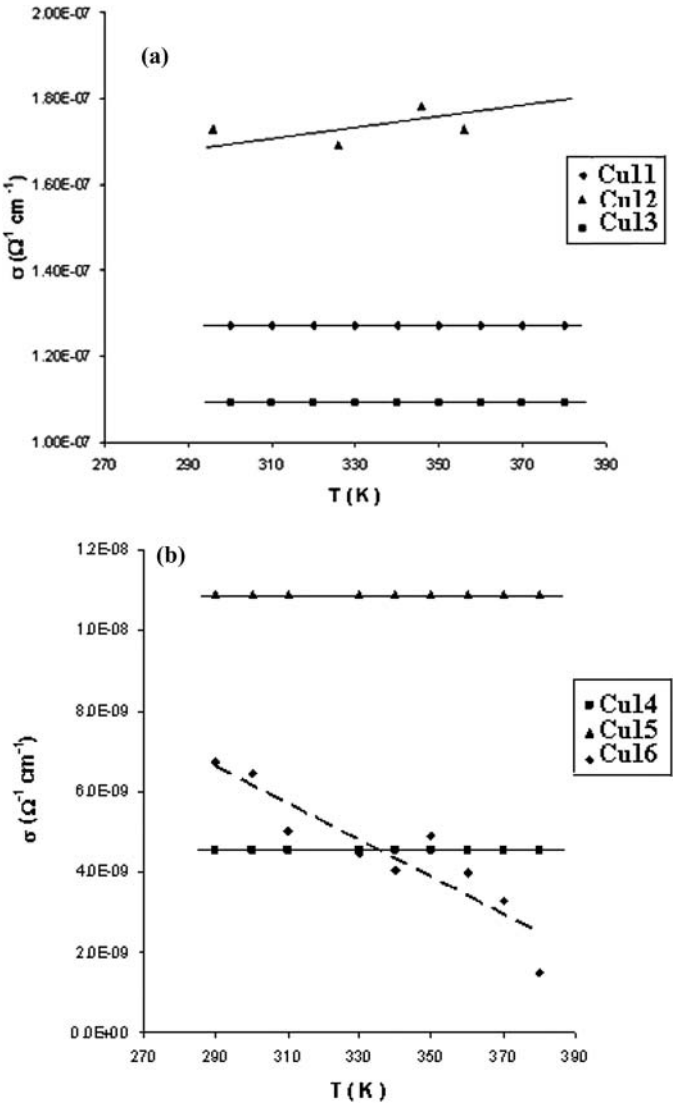

Fig. 16. Temperature dependence of dc electrical conductivity for polymers: (a) **Cu11**–**Cu13**; (b) **Cu14**–**Cu16**.

4 Conclusions

Narrow-sized spherical aramides nanoparticles containing pyridine have been successfully prepared by ultrasonication of aromatic acids chlorides namely; isophthaloyl, pyridine-3,5-dicarbonyl and pyridine-2,6-pyridine-dicarbonyl dichlorides with the isomeric diamines in dioxane/water (100/5 v/v). All polymers prepared in such reaction condition were well-separated spherical particles with some interconnection degree as judged by SEM images. The average diameter of the particles ranges from 50–98 nm. Particles of pyridine containing polymers exhibited large diameter compared to their phenylene counterpart and this result could be attributed to their tendency to form a relatively higher number of H-bonding interactions. Thermal analyses data demonstrated similar major amide linkage degradation and the T_d value of phenylene-containing polymers at 28% weight loss was 400°C, which is comparable as those of high molecular-weight polymeric fiber of this chemical structure. Linear wholly symmetric meta-polymers showed relatively higher η_{inh} and thermal stability and thus, higher degree of polymerization than their nonsymmetrical counterparts. Copper (II) ions were complexed with these polymers in a (1:2) ratio and the structures of the complexes are proposed on the basis of their IR, UV, ESR and elemental analyses data. Pyridine-containing polymers Cu12, Cu13 and Cu14, Cu16 showed similar sites of metal coordination and hence the metal ion accommodates inside the inner cavity made by the pyridine nitrogen atom with two hydrogen amide atoms pointing towards the cavity while the carbonyl groups are directed outside of the inner cavity producing five- and six-membered chelate rings, respectively. The appearance of the sharp (Cu-N) bands at υ 678 and υ 680 cm^{-1} in these complexes unambiguously proved that the pyridine nitrogen atom represents the central binding site. The ERS spectra of the copper compounds state at room temperature are quite similar and exhibited typical axial spectra with $g_{//}$and $g_{\perp}$ features and the data indicated that complexes **Cu11–Cu14** and **Cu16** have square planner geometry while **Cu15** has a six coordinate octahedral geometry. The thermal properties of the prepared polymeric complexes were evaluated by DTG, TGA and DSC techniques and results revealed their high thermal stabilities. Thermal analysis data of this series demonstrated similar major amide linkage degradation and polyamides-containing pyridine **Cu12**, **Cu15** exhibited the highest thermal stability. The total mass loss values of this polymers series proved the loss of nearly 40–48% of masses throughout the entire thermal stages up to 700°C and structures of the remaining residues further confirm the reported compositions. Based on polymer structural variations, the incorporation of copper into the polymers backbones significantly improved the optical and thermal properties. The dc electrical conductivity results of polymers **Cu11–Cu16** revealed different behaviors and it is obvious that the polymer structural variations play a major role in determining the electrical conduction efficiency of the complexes. The dc conductivity of pyridine-containing polymers **Cu12**, **Cu15** exhibited higher σ values compared to other analogues. These types of nano-sized polymeric aramides and their copper complexes may find some applications as new semiconducting nanoparticles.

Acknowledgments

Financial support by Alexandria University-Research Enhancement Program (ALEXREP) grant no. (HLTH-08-01) is gratefully acknowledged.

References

1. García, J.M., García, F.C., Serna, F.C. and de la Peña, J.L. (2010) *Prog. Polym. Sci*., 35, 623–86.
2. Alvarez, J.C., Campa, J.G., Lozano, A.E. and Abajo, J. (2001) *Macromol. Chem. Phys*., 202, 3142–3148.
3. Tamami, B. and Yeganeh, H. (2001) *Polymer*, 42, 415–420.
4. Oishi, Y., Kakimoto, M. and Imai, Y. (1988) *Macromolecules*, 21, 547–550.
5. Liou, G.S. and Hsiao, S.H. (2002) *J. Polym. Sci. Part A Polym. Chem*., 40, 2564–2574.
6. Pourjavadi, A., Zamanlu, M.R. and Zohuriaan-Mehr, M. J. (1999) *Angew. Makromol. Chem*., 269, 54–60.
7. Hearle, J.W.S. High Performance Fibers. Woodhead Publishing Ltd.: Cambridge, UK, 2001.
8. Nelson, G.L. and Wilkie, C.A. (2003) Fire and Polymers. Washington D.C., USA: American Chemical Society.
9. Odian, G. Principles of Polymerization. John Wiley & Sons Ltd.: New Jersey, 2004.
10. Alvarez, J.C., de la Campa, J.G., Lozano, A.E. and de Abajo, J. (2001) *Macromol. Chem. Phys*., 202, 3142–3148.
11. Spiliopoulos, I.K. and Mikroyannidis, J.A. (1998) *Macromolecules*, 31, 1236–1245.
12. Eastmond, G.C., Paprotny, J. and Irwin, R.S. (1999) *Polymer*, 40, 469–486.
13. Liou, G.S., Hsiao, S.H., Ishida, M., Kakimoto, M. and Imai, Y. (2002) *J. Polym. Sci., Part A: Polym. Chem*., 40, 2810–2818.
14. Hsiao, S.H. and Chen, W.T. (2003) *J. Polym. Sci., Part A: Polym. Chem*., 41, 420–431.
15. Odriozola, I., Kyritsakas, N. and Lehn, J.M. (2004) *Chem. Commun*., 62–63.
16. Berl, V., Huc, I., Khoury, R.G. and Lehn, J.M. (2001) *Chem. Eur. J*., 7, 2810–2820.
17. For reviews: Special issue on Molecular Machines (Stoddard, J.F, Guest Ed..) (2001) *Acc. Chem. Res*., 34, 409; Balzani, V., Credi, F., Raymo, M., Stoddard, J.F. (2000) *Angew. Chem., Int. Ed*., 39, 3348–3391.
18. Mohy Eldin, M.S., Shoroen, C.G.P.H., Janssen, A.E.M., Mita, D.G. and Tramper, J. (2000) *J Mol. Catal. B. Enzym*., 10, 445–451.
19. Ni, H. and Kawaguchi, H. (2004) *J. Polym. Sci. Part A: Polym. Chem*., 42, 2833–2844.
20. Lin, C., Zang, Z., Zheng, J., Liu, M. and Zhu, X.X. (2004) *Macromol. Rapid Commun*., 25, 1719-1723.
21. Vennes, M. and Zentel, R. (2004) *Macromol. Chem. Phys*., 205, 2303–2311.
22. Huang, X. and Brittain, W.J. (2001) *Macromolecules*, 34, 3255–3260.
23. Imbert-Laurenceau, E., Berger, M.C., Pavon-Djavid, G., Jouan, A. and Migonney, V. (2005) *Polymer*, 46, 1277–1285.
24. Hassan, H.H.A.M., Elhusseiny, A.F. and Sweyllam, A.M. (2010) *J. Macromol. Sci. Part* A, 47, 521–533.
25. Jain, S.L., Bhattacharyya, P., Milton, H.L., Slawin, A.M.Z., Crayston, J.A. and Wollines, J.D. (2004) *Dalton Trans*., 862–871.
26. (a) Ge, Z., Yang, S., Tao, Z., Liu, J. and Fan, L. (2004) *Polymer*, 45, 3627–3635; (b) Tamami, B., Yeganeh, H. (2002) *Eur. Polym. J*., 38, 933–940.
27. Coats A.W. and Redfern J.P. (1961) *Nature*, 201, 68–69.
28. Johnson, D.W. and Gallagher, P.K. (1972) *J. Phys. Chem.,* 76, 1474–1479.
29. Kokta, B.V., Valade, J.L. and Martin, W.N. (1973) *J. Appl. Polym. Sci*., 17, 1–19.
30. Singh, B.K., Jetley, U.K., Sharma, R.K. and Garg, B.S. (2007) *Spectrochim. Acta Part A*, 68, 63–73.
31. (a) Ruiz, R., Sanz, J., Lloret, F., Julve, M., Faus, J., Bois, C. and Munoz, M. C. (1993) *J. Chem. Soc. Dalton Trans*, 3035–3039; (b) Karaboecek, S. and Karaboecek, N. (1997) Polyhedron, 11, 1771–1774.
32. Hathaway, B.J. and Billing, D.E. (1970) *Coord. Chem. Rev*., 5, 143–207.
33. Ruf, M., Noll, B., Groner, M., Yee, G.T. and Pierpont, C.G. (1997) *Inorg. Chem*., 36, 4860–4865.
34. Marrwaha, S.S., Kaur, J. and Sodhi, G.J. (1994) *J. Inorg. Biochem*., 54, 67–74.
35. Skotheim, T.A., Elsenbaumer, R.L. and Reynolds, J.R. Handbook of Conducting Polymers. Marcel-Dekker: New York, 1998.
36. Mott, N.F., Davis, E. Electronic Processes in Non-Crystalline Materials, Clarendon Press: Oxford, 1979.